Optical conductivity of the t_{2g} two-dimensional electron gas

Ming Xie, Guru Khalsa, and A. H. MacDonald
Department of Physics, University of Texas at Austin, Austin, Texas 78712-1081, USA
(Received 5 August 2013; revised manuscript received 2 June 2014; published 12 June 2014)

Motivated by recent interest in perovskite surfaces and heterostructures, we present a theoretical analysis of the optical conductivity of a two-dimensional electron gas (2DEG) formed in the t_{2g} bands of an oxide with perovskite structure based on the Kubo formula and a realistic electronic structure model. We find that, when the electric field is polarized in the plane of the 2DEG, the optical conductivity is dominated by nearly independent Drude contributions from all occupied two-dimensional subbands, whereas for perpendicular-to-plane polarization it has strong intersubband features. For perpendicular-to-plane polarization, Coulomb interactions couple different intersubband modes, transferring spectral weight to higher energy absorption features and inducing a strong excitation that is collective in nature. Our analysis suggests that perpendicular-to-plane optical conductivity studies may help advance understanding of the roles of lattice distortions and electron-electron interactions in complex oxide 2DEG quantum confinement physics.

DOI: 10.1103/PhysRevB.89.245417 PACS number(s): 78.68.+m, 73.20.−r, 68.47.Gh, 73.40.−c

I. INTRODUCTION

Heterostructures and multilayers based on the perovskite lattice have recently been the focus of an enormous research effort. The perovskite lattice structure is formed by compounds containing elements across much of the periodic table [1] and can be grown epitaxially with very high quality [2]. Perovskite heterointerfaces often have properties that are drastically distinct from those of their parent bulk materials. The most well known example of this tendency is the polar/nonpolar interface [3] between the band insulators $LaAlO_3$ and $SrTiO_3$ which hosts a high mobility two-dimensional electron gas (2DEG), formed mainly from the t_{2g} orbitals of $SrTiO_3$, that can be magnetic [4] or superconducting [5] or both [6]. There have by now been many studies of $SrTiO_3$ t_{2g} 2DEGs formed at various interfaces and surfaces [7–11]. 2DEGs that are mostly similar in character but have much stronger spin-orbit (SO) coupling can be formed at $KTaO_3$ interfaces and surfaces [12,13]. In both $SrTiO_3$ and $KTaO_3$, it has been shown that, because of strong and nonlinear dielectric response at low temperature, the 2DEGs consist of a high electron density component containing mostly electrons that are strongly confined near a surface or interface, and a low-density tail component consisting of weakly confined electrons that occupy closely spaced subbands which extend ∼10–20 nm into the bulk of the material [14,15].

Optical studies have played an important role in conventional semiconductor 2DEGs [16,17]. Absorption of light with electric fields polarized perpendicular to the 2DEG plane has been especially valuable because it measures intersubband optical transition energies and in this way characterizes 2DEG quantum confinement. No intersubband optical response is observed [18] when light is polarized with its electric field in the 2DEG plane. Because optical spectra can probe intersubband transition energies, optical characterization also has the potential to play an important role in sorting out the quantum confinement physics in t_{2g} 2DEGs. Experimental guidance would be especially valuable because of the complicating influence in the oxide case of nonlinear dielectric screening, and because of the greater likelihood of structural distortions and defects at interfaces.

In this article we explore the optical conductivity of t_{2g} 2DEGs theoretically, with a view toward shedding light on the information which can be garnered from future experimental studies [19]. We find that the optical response of the t_{2g} 2DEG is dominated by electrons within the first few layers of the surface or interface. When light is polarized in the 2D plane, the conductivity is dominated by a Drude peak to which all occupied t_{2g} orbitals contribute. The integrated strength of this peak provides information on the carrier density which is complementary to that available from Hall effect measurements. There are, however, weak intersubband peaks which could be very revealing if they could be detected. Measurements of the peak frequencies should be very valuable in constraining confinement models. The corresponding peak strengths are sensitive to hybridization between different t_{2g} orbitals, which is weak in the ideal cubic case, and may therefore shed light on spin-orbit coupling strengths and on structural distortions of the pseudocubic cell near the interface. For light polarized perpendicular to plane, the optical conductivity has strong intersubband features related to hopping amplitudes perpendicular to the interface, and to the confining potential. When a t_{2g} 2DEG responds to an *ac* field perpendicular to the interface, the charge density and therefore the confinement potential also respond. These Coulombic effects produce a depolarization effect which must be accounted for self-consistently. We show that depolarization effects shift spectral features and that, depending on the 2DEG density, they can result in sharp plasmonic excitations.

Our paper is organized as follows. In Secs. II and III below we briefly discuss the model we use for a t_{2g} 2DEG and comment on the Kubo formula expressions we use for the conductivity. Our main results are presented and discussed in Sec. IV. Section V explains our random-phase-approximation treatment of the depolarization effect and discusses its influence on the response of the 2DEG to a perpendicular-to-plane field. The paper concludes in Sec. VI with a brief summary and conclusions.

II. MODEL

In the perovskite ABO_3 unit cell, the B cation is surrounded by an octahedral oxygen cage which lifts its d-orbital degeneracy, pushing the $e_g = \{x^2 - y^2, 3z^2\}$ levels up relative to the $t_{2g} = \{yz, zx, xy\}$ levels. We focus on systems with conduction bands that have t_{2g} character and are well separated from oxygen p-orbital derived valance bands. In a cubic environment, the yz, zx, and xy members of the t_{2g} manifold are very weakly hybridized. Under most circumstances atomic-like SO coupling is the dominant source of hybridization. When it is neglected, the three orbitals therefore contribute essentially independently to physical properties of the 2DEG, which we assume forms in x-y planes. The symmetries which lead to this circumstance can be understood by considering a two-center approximation description in which an xy electron hops along the x direction within a BO_2 plane from a B atom xy orbital to another B atom via π bonding to the p_y orbital of the intermediate oxygen atom that is virtually occupied. We define this and other symmetry equivalent metal to metal effective hopping amplitudes as $-t$. For hopping in the y direction, the B atom xy orbital hops through an oxygen p_x orbital to a neighboring B atom xy orbital with the same effective hopping amplitude. There is also a smaller but still important z-direction hopping amplitude $-t'$ for xy orbitals which connects one BO_2 layer to another that is closer to or further from the interface. $\{yz,zx\}$ orbitals, on the other hand, have strong $(-t)$ out-of-plane hopping and weak hopping $(-t')$ in one of two in-plane directions. These orbital conserving hopping processes are responsible for most of the qualitative properties of t_{2g} 2DEGs and are readily expressed mathematically by the system's tight binding model Hamiltonian.

For a single BO_2 layer, the tight-binding Hamiltonian within the t_{2g} subspace is

$$H_{SL} = \sum_{\vec{k},\gamma,\sigma} \epsilon_\gamma(\vec{k}) \hat{n}_{\vec{k},\gamma,\sigma}, \tag{1}$$

where $\vec{k}$ is the in-plane crystal momentum, $\gamma = \{yz,zx,xy\}$, and σ is the spin index. The $\epsilon_\gamma(\vec{k})$ are defined by

$$\begin{aligned} \epsilon_{yz}(\vec{k}) &= -2t' \cos(k_x a) - 2t \cos(k_y a) \\ \epsilon_{zx}(\vec{k}) &= -2t \cos(k_x a) - 2t' \cos(k_y a) \\ \epsilon_{xy}(\vec{k}) &= -2t \cos(k_x a) - 2t \cos(k_y a) \end{aligned} \tag{2}$$

where a is the lattice constant. Similarly the interlayer coupling Hamiltonian is

$$H_{\text{inter}} = -\sum_{\langle l,l'\rangle,\gamma,\sigma} t_{\gamma,z}\, \hat{c}^\dagger_{\vec{k},l,\gamma,\sigma} \hat{c}_{\vec{k},l',\gamma,\sigma}, \tag{3}$$

where $\langle l,l'\rangle$ are neighboring layers, $t_{\gamma,z} = t'$ for $\gamma = xy$, and $t_{\gamma,z} = t$ for $\gamma = \{yz,zx\}$ are hopping parameters in the z direction. Spin-orbit coupling of the cation d orbitals is mainly atomic in character. In the calculations described below we have used a model [14] in which we project atomic spin-orbit coupling onto the t_{2g} space. The corresponding Hamiltonian takes the form

$$H_{\text{SO}} = \frac{\Delta_{\text{SO}}}{3} \begin{pmatrix} 0 & i & 0 & 0 & 0 & -1 \\ -i & 0 & 0 & 0 & 0 & i \\ 0 & 0 & 0 & 1 & -i & 0 \\ 0 & 0 & 1 & 0 & -i & 0 \\ 0 & 0 & i & i & 0 & 0 \\ -1 & -i & 0 & 0 & 0 & 0 \end{pmatrix} \begin{Bmatrix} yz,\uparrow \\ zx,\uparrow \\ xy,\uparrow \\ yz,\downarrow \\ zx,\downarrow \\ xy,\downarrow \end{Bmatrix}, \tag{4}$$

where Δ_{SO} is the interaction strength parameter. Note that, although this model contains spin-orbit coupling, it does not capture the processes which can lead to Rashba [13] spin-orbit induced momentum-splitting of the Bloch band's double spin degeneracy.

Most t_{2g} 2DEGs are formed near the surface of a sample and sit on a grounded substrate. It follows that the the electric field must vanish in the bulk of the substrate, far below the surface. The Poisson equation then implies that the electric field above the 2DEG is proportional to the electron density. The electric field in the region occupied by the 2DEG is screened both by the 2DEG electrons and by distortions of the ionic host lattice. The extremely strong dielectric response of the host material is related to its soft optical phonon modes, which involve nearly rigid displacements of the central Ti atoms relative to their oxygen octahedra. The strong response occurs only for relatively weak electric fields and only at relatively long wavelengths exceeding several nanometers. A simple model which qualitatively accounts for this complex physical situation has been described previously in Ref. [14]. Specifically, the electric field distribution is determined by solving coupled Poisson-Schrodinger equations in which both electron densities and anharmonic polar lattice displacements contribute to the electrostatic potential. Our linear response calculations start from a ground state with t_{2g} subbands calculated using the confinement model explained in Ref. [14] and forcing the 2DEG to lie within the first 60 metal layers. We are confident that this model is realistic enough to capture qualitative features of the linear response. Our goal is to provide a framework for interpreting optical absorption measurements in order to gain a more detailed understanding of 2DEG properties.

Because t_{2g} 2DEGs can be prepared over a very wide density range, we have considered the three representative areal density n regimes identified in Ref. [14], referred to below as "low" ($n = 2.3 \times 10^{13}$ cm^{-2}), "medium" ($n = 2.0 \times 10^{14}$ cm^{-2}), and "high" ($n = 5.9 \times 10^{14}$ cm^{-2}) densities. In all three cases the electrons are distributed across many layers. A high density region emerges in the first few BO_2 atomic layers in the medium and high density cases. The extended low-density tails, present because of $SrTiO_3$'s extremely large linear dielectric constant, are mostly $\{yz,zy\}$ in character. In the higher density cases, a substantial fraction of electrons occupy the lowest energy subband which is also mostly xy in character; xy electrons are more readily confined than $\{yz,zy\}$ electrons because of their weak hopping along the z direction. The present calculations are motivated by the expectation that quantitative comparisons between experiment and this simple theoretical model can be used to refine approximations and improve theoretical predictive power.

III. LINEAR RESPONSE THEORY

We consider the response of the 2DEG current to a weak external electromagnetic field. In the random phase approximation, the conductivity tensor is given by the well known Kubo formula [20]

$$\sigma_{\alpha\beta}(\omega) = i\hbar \sum_{m,n,\vec{k}} \left(\frac{f_n - f_m}{\epsilon_m - \epsilon_n} \right) \frac{\langle m,\vec{k}|\hat{j}_\alpha|n,\vec{k}\rangle\langle n,\vec{k}|\hat{j}_\beta|m,\vec{k}\rangle}{\hbar\omega - (\epsilon_m - \epsilon_n) + i\eta} \quad (5)$$

where m,n are band and α,β Cartesian direction indices, $\vec{k}$ is the 2DEG crystal momentum, and $\hat{j}_\alpha$ is the paramagnetic component of the current operator for which an explicit expression is given below. The dependence of the Fermi distribution function f_n and the band energy ϵ_n on $\vec{k}$ is left implicit for notational simplicity. The ratio of Fermi factor to energy differences should be understood as a derivative in the $m = n$ limit so that the intraband contribution to the conductivity is

$$\sigma^{IB}_{\alpha\beta}(\omega) = i\hbar \sum_{n,\vec{k}} \left(-\frac{\partial f}{\partial \epsilon} \right) \frac{\langle n,\vec{k}|\hat{j}_\alpha|n,\vec{k}\rangle\langle n,\vec{k}|\hat{j}_\beta|n,\vec{k}\rangle}{\hbar\omega + i\eta}. \quad (6)$$

We treat $\eta = \hbar\tau^{-1}$ as a phenomenological parameter which accounts for the Bloch state lifetimes, assigning it a value that is independent of band index.

In Eq. (5) we have taken the limit $q \to 0$ because the wavelengths of optical frequency electromagnetic waves are long compared to Fermi wavelengths. The paramagnetic current operator [21] is therefore given by the commutator of the Hamiltonian with the polarization operator $\hat{P}$:

$$\hat{j}_\alpha = -\frac{ie}{\hbar}[H, \hat{P}_\alpha]. \quad (7)$$

In the tight binding approximation, electrons are considered to sit on lattice sites so position is discrete in real space. The polarization operator therefore takes the form $\hat{P} = \sum_i \vec{R}_i \hat{n}_i$, where $\vec{R}_i$ is the position operator and $\hat{n}_i$ the total number operator at site i. It follows that evaluating the commutator of H with $\hat{P}$ is essentially equivalent to differentiating it with respect to wave vector. Therefore only the $\vec{k}$ dependent part of the Hamiltonian contributes to the in-plane current operator. We find, from Eqs. (1) and (2), that the x-direction current operator is spin independent, diagonal in layer, and given in a $\{yz,zx,xy\}$ representation by

$$\hat{j}_x = \frac{e}{\hbar}\frac{\partial H}{\partial k_x} = \frac{ea}{\hbar} \begin{pmatrix} -2t' \sin(k_x a) & 0 & 0 \\ 0 & -2t \sin(k_x a) & 0 \\ 0 & 0 & -2t \sin(k_x a) \end{pmatrix}. \quad (8)$$

Note that the in-plane current operator couples only subbands with the same orbital character and that its action is independent of position relative to the interface. In the absence of orbital hybridization (due to SO coupling in the model we considered) the bare Hamiltonian is also diagonal in orbital. It follows that in this case there are no intersubband transition contributions to the in-plane conductivity, either from transitions between subbands with the same orbital character or from transitions between subbands with different orbital character. When hybridization is neglected the in-plane orbital conductivity has only a Drude response centered on $\omega \to 0$.

Because the system is finite in the z direction, the commutator in Eq. (7) is best evaluated in position space for this current component. We find that

$$\hat{j}_z = -\frac{ie}{\hbar} \sum_{\vec{k},l,\gamma} a t_{\gamma,z} (\hat{c}^\dagger_{\vec{k},l+1,\gamma} \hat{c}_{\vec{k},l,\gamma} - \hat{c}^\dagger_{\vec{k},l-1,\gamma} \hat{c}_{\vec{k},l,\gamma}), \quad (9)$$

where $t_{\gamma,z} = \{t,t,t'\}$ for hopping in the z direction in the $\{yz,zx,xy\}$ basis. Because j_z is off-diagonal in layer index, optical transitions between different subbands with the same orbital character are allowed even in the absence of interorbital hybridization. Although orbital hybridization can weakly allow additional optical transitions, intraorbital contributions dominate the perpendicular-to-plane optical response, especially so when the Fermi energy is much larger than the SO splitting. For the calculations presented below this criterion is satisfied at medium and high densities.

The real part of the longitudinal conductivity tensor satisfies certain sum rules which are useful for verifying numerical results and also potentially useful in interpreting experiments. These sum rules limit conductivity contributions from intersubband transitions. By employing the commutation relation (7), we obtain the following sum rules for in-plane and perpendicular-to-plane conductivity tensors:

$$\int_{-\infty}^{\infty} d\omega\, \mathrm{Re}[\sigma_{xx}(\omega)] = \frac{\pi e^2}{\hbar^2} \sum_{n,\vec{k}} \langle n\vec{k}| \frac{\partial^2 H}{\partial k_x^2} |n\vec{k}\rangle f_n \approx \pi e^2 \sum_n \frac{n_n}{m^*_{xx,n}} \quad (10)$$

and

$$\int_{-\infty}^{\infty} d\omega\, \mathrm{Re}[\sigma_{zz}(\omega)] = -\frac{i\pi e}{\hbar} \sum_{n,\vec{k}} \langle n\vec{k}|[\hat{j}_z, \hat{P}_z]|n\vec{k}\rangle f_n. \quad (11)$$

In Eq. (10), the second form for the right-hand side becomes exact when the largest Fermi wave vector is far from the BZ boundary so that the parabolic approximation for band dispersion is accurate. Here n_n corresponds to the density of the nth band. In this limit we therefore recover the standard result that, when integrated over frequency, the contribution of a band to the optical conductivity is proportional to the density of electrons in that band scaled by the inverse effective mass. In cases when orbital hybridization effects are weak, that is, SO coupling and structural distortions are small, the second form for Eq. (10) may be simplified to

$$\frac{2\pi e^2 a^2}{\hbar^2} \sum_\gamma t_{\gamma,x} n_\gamma, \quad (12)$$

where n_γ is the total density associated with electrons of orbital character γ and corresponding hopping parameters in the x direction, $t_{\gamma,x}$.

The commutator in Eq. (11) is

$$\frac{iea^2}{\hbar}\sum_{\vec{k},l,\gamma} t_{\gamma,z}(\hat{c}^{\dagger}_{\vec{k},l+1,\gamma}\hat{c}_{\vec{k},l,\gamma} + \hat{c}^{\dagger}_{\vec{k},l-1,\gamma}\hat{c}_{\vec{k},l,\gamma}). \qquad (13)$$

Contributions to Eq. (11) are therefore directly proportional to the amplitude for an electron in layer l to hop to a neighboring layer, $l \pm 1$.

IV. RESULT AND DISCUSSION

In this section, we report on and discuss results for the optical conductivity of the $SrTiO_3$ surface 2DEG models described in Sec. II. The hopping parameters t and t' were taken to have the values [22] 236 meV and 35 meV respectively and the lattice constant a was set to 3.904 Å. Figure 1 shows the real part of the in-plane optical conductivity for $\hbar\omega$ up to 200 meV, including both the Drude conductivity and the intersubband part of the conductivity, calculated with a phenomenological energy uncertainty $\eta = 10$ meV to account for disorder scattering. This value of η yields Drude peak heights consistent with recent dc resistivity measurements [23]. The Drude conductivity increases monotonically with the density of the 2DEG as expected on the basis of the sum rules discussed above. The in-plane optical conductivity is dominated by the Drude contribution at all densities.

From Eq. (2) the xy and zx band masses along the x direction are smaller than the yz mass (by a factor $\sim$10). This suggests that, in this limit, the Drude weight will typically be dominated by the xy and zx pocket contributions. It is common in experiment to infer carrier density on the basis of sum rules and assumed values for the effective mass. By evaluating the total sum rule in our calculation as a function of carrier density, we can express our theoretical results for the Drude weight as a function of density in terms of a density-dependent sum-rule effective mass. In Table I we see that this mass drops as the carrier density increases and the contribution of the lowest xy subband becomes more dominant. Experimentally the carrier density can be estimated on the basis of Hall effect measurements, although interpretation may be complicated by the presence of the complicated band structure in these material systems. Simultaneous measurements of Drude weight and Hall conductivity, combined with these sum-rule effective masses could be helpful in checking the consistency of carrier density estimates.

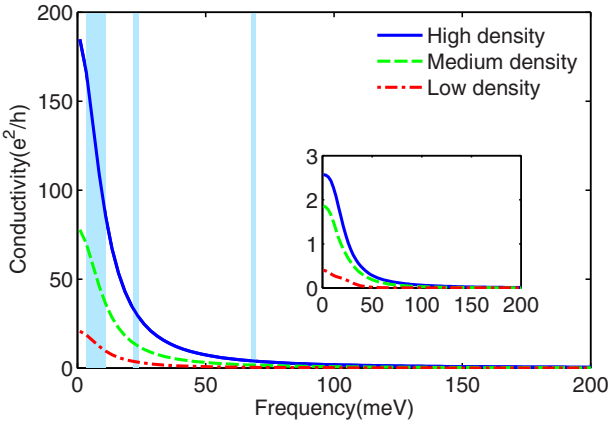

FIG. 1. (Color online) In-plane optical conductivity of a $SrTiO_3$ 2DEG in e^2/h units for light polarized in the plane of the t_{2g} 2DEG at high (5.9×10^{-14} cm^{-2}), medium (2×10^{-14} cm^{-2}), and low (2.3×10^{-13} cm^{-2}) carrier densities as defined in Ref. [14]. The strength of the spin-orbit coupling Δ_{SO} is set to 18 meV. The shaded region in the figure highlights the frequency region in which the electronic conductivity is expected to be obscured by optical phonons. η has been set to 10 meV in order to yield $\omega \to 0$ limits that are similar to those observed experimentally. The inset shows the intersubband contribution to the conductivity, due mainly to optical transitions from the low-density tail.

TABLE I. Estimates of averaged inverse effective masses from the integrated Drude weight. The hopping parameters t and t' could be converted to inverse effective masses $m_e/m_L = 0.94$ and $m_e/m_H = 0.14$, respectively. The averaged inverse effective masses fall between these values corresponding to the limiting cases when only the light mass (m_L) bands or the heavy mass (m_H) bands are populated. m_e is the bare electron mass.

Density (cm^{-2})	Integrated Drude weight (e^2cm$^{-2}/m_e$)	Inverse effective mass (m_e/m^*_{xx})
5.9×10^{14}	1.15×10^{15}	0.62
2.0×10^{14}	4.65×10^{14}	0.69
2.3×10^{13}	5.16×10^{13}	0.71

As shown in the inset in Fig. 1 there is a small intersubband contribution to the conductivity which originates from the low-density tail states. For these states, subband separations are comparable to spin-orbit coupling strengths ($\Delta_{SO} = 18$ meV) allowing for considerable orbital hybridization. The intersubband contribution will likely be difficult to isolate experimentally because it is weak in a relative sense. Additionally, because of the small band separations of tail states it will be difficult to separate spectrally from the Drude peak at typical values of η because it is also peaked close to $\omega = 0$. Intersubband features might be observable in systems with spin-orbit coupling strengths that are larger than those of $SrTiO_3$ ($\Delta_{SO} = 18$ meV) or in systems with substantially smaller lifetime broadening than is currently achievable (see below). We also note that, in absence of spin orbit coupling, the matrix elements remain diagonal in the orbital basis as well as the subband basis. In this case the intersubband contribution vanishes.

We remark that the utility of optical conductivity measurements as a probe of electronic properties is mitigated by the presence of strong optical phonon contributions. In Fig. 1 we have shaded the frequency ranges expected [24] to be obscured by the three optical phonon modes which overlap with 2DEG energy scales. The frequency of the low-energy phonon at the $\vec{q} = 0$ is strongly dependent on temperature. To represent this we have included a shaded region spanning its temperature dependence.

In t_{2g} 2DEG systems with strong spin-orbit coupling, spectral features associated with transitions between strongly confined orbitals may become visible. A promising candidate of such systems is the 2DEG formed at the gated surface of the 5d transition-metal oxide $KTaO_3$ [12] which has the same

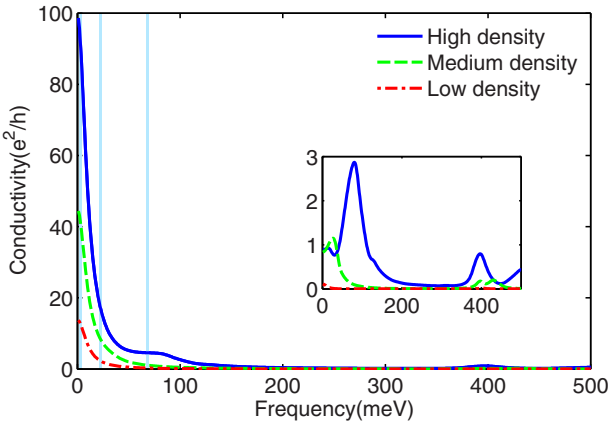

FIG. 2. (Color online) In-plane optical conductivity of a t_{2g} 2DEG with strong atomic spin-orbit coupling with strength $\Delta_{SO} = 400$ meV. The inset plots the intersubband part only. η has been set to 10 meV.

orbital makeup except there the spin-orbit split energy has been observed to be as large as 400 meV. To illustrate this effect, we have artificially set the atomic spin-orbit coupling strength parameter $\Delta_{SO} = 400$ meV in the $SrTiO_3$ 2DEG model and repeated the in-plane optical response calculation. In Fig. 2 we see that transitions within the weakly confined subbands are again obscured because of the Bloch state lifetime. Now, however, the spin-orbit coupling strength is strong enough to induce appreciable hybridization of the strongly confined subbands. The inset of Fig. 2 again shows the intersubband optical response features are most prominent at high carrier densities. The strongest feature is a broad peak centered at ∼400 meV associated with transitions to bulk spin-orbit split bands near the bottom of the conduction band. It is present at all carrier densities, but stronger at higher carrier densities. A second feature associated with the confinement energy scale is now allowed because of orbital hybridization within the t_{2g} manifold. Even in the high density case, the 400 meV SO coupling is larger than the confinement energy of the lowest subband. This suggests that all bands have strongly hybridized t_{2g} character. We emphasize that, since the SO coupling is local, it does not contribute to the current operator. Therefore, the matrix elements of the current operator in the optical conductivity still favor xy and zx orbitals due to their strong bonding in the x direction. The peak at ∼80 meV is dominated by a peak in the zx projected density of states related to the confinement energy of the most confined $\{yz,zx\}$ bands. Because the energy scales associated with structural deformations (of the parent material or induced by the interface) are not expected to be this large [25], we conclude that in the absence of large SO coupling in plane conductivity measurements are unlikely to provide useful information.

Typical perpendicular-to-plane response is illustrated in Fig. 3. In this case the current operator is diagonal in orbital, but not diagonal in subband. We therefore see a number of strong spectral features as summarized in Fig. 3(a). At low carrier density, the subband splittings are not much larger than the lifetime broadening η and features associated with allowed transitions are therefore obscured in Fig. 3(a). In practice, however, low carrier density t_{2g} 2DEGs tend to have higher mobilities, and therefore smaller values of η, so the situation depicted in Fig. 3(a) may be too pessimistic. At our medium density, a peak emerges at ∼40 meV (labeled M1) that is associated with an optical transition from the lowest occupied $\{yz,zx\}$ subband to the second lowest $\{yz,zx\}$ subband. The transitions to the many nearby unoccupied subbands of $\{yz,zx\}$ character give the peak a broad line shape. In Fig. 3(b) we show the electronic structure which yields these conductivities. The $\{yz,zx\}$ transitions are prominent because these bands have a large mass in one direction and therefore a larger density of states than the xy bands, and also because the z-direction current operator is proportional to their larger interlayer hopping amplitudes. We have highlighted

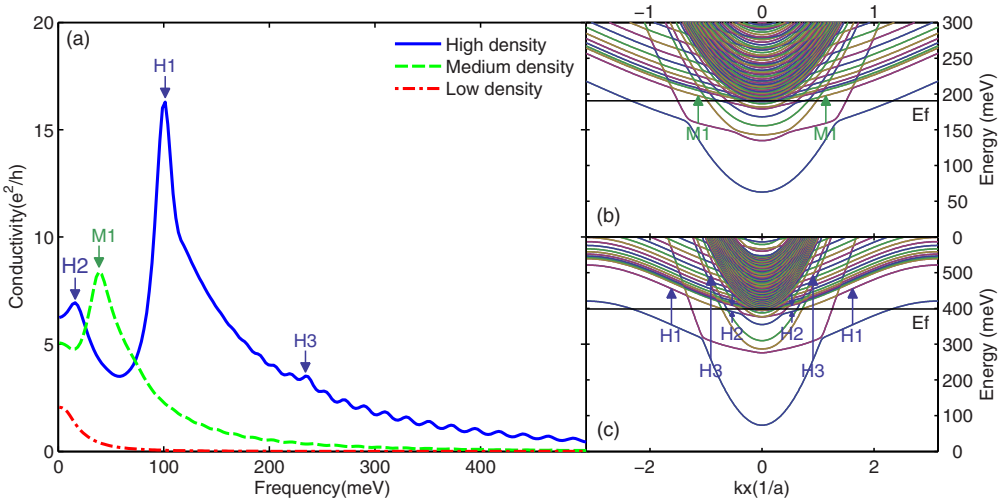

FIG. 3. (Color online) (a) Perpendicular-to-plane optical conductivities for low, medium, and high densities. (b) Self-consistent band structure for a density of 2×10^{14} cm^{-2}. (c) Self-consistent 2DEG subband structure for a density of 5.9×10^{14} cm^{-2}. The main optical transitions for perpendicular-to-plane polarization are indicated by color-coordinated arrows in the conductivity and band-structure plots. The subbands contributing to the feature labeled H2 are too close to be seen easily in (c) and have been denoted with two arrows for clarity. The disorder-broadening η has been set to 10 meV.

the transitions responsible for the ∼40 meV peak with green arrows in Fig. 3(b).

For high densities, we see two features at ∼16 and ∼100 meV. We identify the higher energy features as originating from the $\{yz,zx\}$ transitions labeled H1 in Fig. 3(c). The H2 feature corresponds to a transition from the second lowest $\{yz,zx\}$ bands to the higher energy $\{yz,zx\}$ bands. The peak labeled H3 has frequency 240 meV and corresponds to the transition from the lowest xy band to the second lowest xy band. It is barely visible because of the weak xy hopping t' in the z direction. These calculations also reveal many small features at higher energies that we associate with transitions between the most strongly confined t_{2g} subbands and the large number of bulk-like bands that are occupied in the 60 layer simulations [14]. These features would become sharper if we performed our calculations with a smaller phenomenological scattering rate η. We expect, however, that in typical systems (which are much larger than 60 unit cells) they will yield a smooth tail in the optical response.

V. DEPOLARIZATION EFFECT

We remark that optical spectroscopy features in conventional semiconductor 2DEGs are shifted from the subband splittings by depolarization effects [16,26]. When electrons transition to unoccupied states, the charge distribution along the z direction is altered, which in turn alters the time-dependent electric field. Similar shifts will occur in oxide 2DEGs. In a two-level system with only the ground level occupied, the peak shift is [26] $2e^2nES/\epsilon$ where n is the density per area of the electrons involved in the transition, E is the subband splitting and S is an effective Coulomb interaction length [26] for the corresponding transition. In the conventional case, intersubband transition energies are small enough that ϵ can be taken to be the static dielectric constant of the host semiconductor material. In the present case many of the transitions of interest involve strongly confined t_{2g} electrons, and have frequencies larger than many of the important optical phonons [see Fig. 3(a) for example]. In our medium-density case, the transition energy falls between optical phonon modes at around 20 and 70 meV. The effective dielectric constant in bulk $SrTiO_3$ in this frequency range is $\epsilon \sim 10$. If we assumed that 10^{14} cm^{-2} $\{yz,zx\}$ electrons are involved in the transition and that the Coulomb interaction length is ∼1 lattice constant, we would estimate that the peak shift is on the order of 190 meV. This simple estimate shows that the depolarization shifts are potentially large. In a system in which several subbands are occupied, the problem becomes more complex because of coupling between different intersubband transitions. In order to account in a complete manner for the depolarization effect, we examine the layer-dependent density-density response function.

To obtain the density-density response function, we first decompose the zz component of the conductivity tensor, σ_{zz}, into contributions from links connecting neighboring layers:

$$\sigma_{LL'}(\omega) = i\hbar \sum_{m,n,\vec{k}} \left(\frac{f_n - f_m}{\epsilon_m - \epsilon_n} \right) \frac{\langle n,\vec{k}|\hat{j}_L|m,\vec{k}\rangle \langle m,\vec{k}|\hat{j}_{L'}|n,\vec{k}\rangle}{\hbar\omega - (\epsilon_m - \epsilon_n) + i\eta} \tag{14}$$

where the uppercase L labels the link between layer l and $l+1$ and L' the link between layer l' and $l'+1$. The current operator j_z is decomposed into currents on each link using

$$\hat{j}_L = -\frac{ie}{\hbar} \sum_{\vec{k},\gamma} a t_\gamma (\hat{c}^\dagger_{\vec{k},l,\gamma} \hat{c}_{\vec{k},l+1,\gamma} - \hat{c}^\dagger_{\vec{k},l+1,\gamma} \hat{c}_{\vec{k},l,\gamma}). \tag{15}$$

It follows that $\sigma_{zz} = \sum_{LL'} \sigma_{LL'}$ and that $\hat{j}_z = \sum_L \hat{j}_L$.

Assuming the system is driven by a monochromatic electric field perpendicular to the surface, the charge density in layer l obeys the continuity equation

$$-iea\omega\rho_l = J_{L-1} - J_L. \tag{16}$$

Here J_L is the expectation value of the current operator on link L and is related to the electric fields on the links by

$$J_L = \sum_{L'} \sigma_{LL'} E_{L'}, \tag{17}$$

where $E_{L'}$ is the electric field on link L'. The density-density response function is defined as

$$\rho_l \equiv \sum_{l'} \chi^0_{ll'} V_{l'}, \tag{18}$$

where $V_{l'}$ is the electric potential on layer l'. Combining Eq. (14) and Eqs. (16)–(18), we arrive at a relation connecting the conductivity and the density-density response function:

$$\chi^0_{ll'} = \frac{1}{ie^2a^2\omega}(\sigma_{L,L'-1} - \sigma_{L-1,L'-1} - \sigma_{L,L'} + \sigma_{L-1,L'}). \tag{19}$$

The superscript "0" indicates it is the response to the total scalar field. The response to the external scalar field is related to χ^0 by the Dyson equation,

$$\chi = (1 - \chi^0 U)^{-1} \chi^0, \tag{20}$$

where U is the two-dimensional Fourier transform of the Coulomb potential in the limit that the 2D momentum $q \to 0$:

$$U_{ll'} = \lim_{q\to 0} \frac{1}{4\pi\epsilon_0} \frac{2\pi e^2}{\epsilon_\infty q} e^{-qa|l-l'|} = \frac{2\pi e^2 a|l-l'|}{4\pi\epsilon_0\epsilon_\infty}. \tag{21}$$

The results for the bare response function χ^0 are illustrated in Fig. 4 where we plot the trace of its imaginary part, which is proportional to spatially integrated absorption in the 2DEG. The spectrum consists of resonances corresponding to transitions between strongly confined t_{2g} subbands, and also resonances which correspond to transitions from confined subbands to the large number of nearly 3D subbands. The main spectral features in this figure can be related to those in the perpendicular-to-plane conductivity plot [Fig. 3(a)], except that the relative strengths of the intersubband transitions are altered. For the high-density case, the first to the second $\{yz,zx\}$ subband transition (labeled H1) continues to be dominant. However, the strength of the first to the second xy subband transition (labeled H3) increases relative to the H1 feature. The transition from the second to the third xy subband is hidden in Fig. 3(a) but becomes visible at 45 meV (between H2 and H1). This trend becomes more significant in

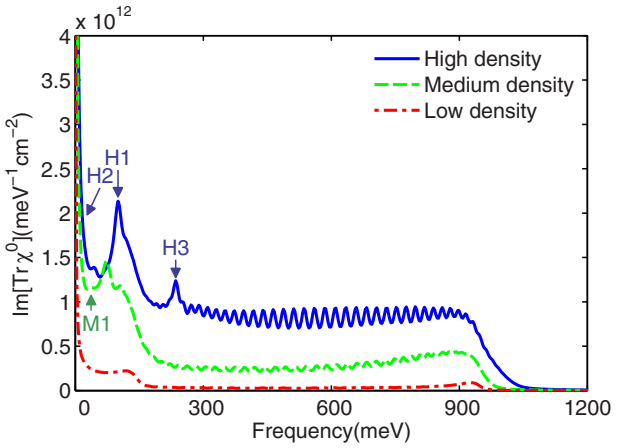

FIG. 4. (Color online) Trace of the imaginary part of the "bare" density-density response function χ^0 for low, medium, and high densities. The features are identified with the transitions labeled in Fig. 3(a). The peaks next to M1 in medium density and next to H1 in high density which are not labeled correspond to xy transitions not visible in Fig. 3(a).

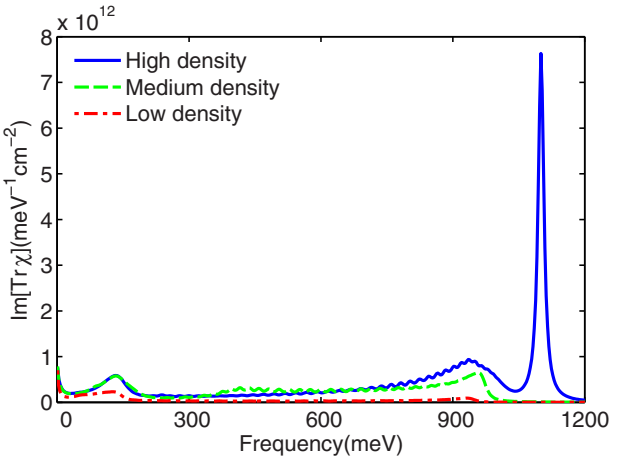

FIG. 5. (Color online) Trace of the imaginary part of the density-density response function χ for low, medium, and high densities.

the medium-density case where the $\{yz,zx\}$ transition M1 can still be identified but has relatively small strength compared to two features at 73 and 103 meV which are not visible in the perpendicular-to-plane conductivity [Fig. 3(a)]. They correspond to transitions from the lowest xy subband to the second and third xy subbands, respectively. Because the current operator in the Kubo formula is proportional to the out-of-plane hopping amplitude $t_{\gamma,z}$, which is much smaller for xy manifold compared to $\{yz,zx\}$ manifold, xy transitions have weaker strength in the optical conductivity spectrum. The densely spaced peaks in the high-frequency part of Fig. 4 correspond to transitions from the most strongly confined t_{2g} subbands to the large number of bulk-like t_{2g} subbands. For subbands of orbital character γ, the upper bound of the intersubband excitations, i.e., the distance between the band edges of the lowest and highest subbands, is $4t_{\gamma,z}$, the width of the dispersion $-2t_{\gamma,z}\cos(k_z a)$ in the bulk, plus the confinement energy, the amount which the lowest subband is pulled down in energy relative to the 3D-like bands. The $\{yz,zx\}$ transitions therefore tend to have a larger upper bound $\sim$1 eV.

Figure 5 shows the results for the response function χ. When the depolarization effect is considered, we see that most of the spectral weight is shifted to higher energies, leaving smooth and weak features at lower energies where intersubband transitions would occur. This behavior is characteristic of systems in which Coulomb interactions couple intersubband transitions, and has been identified previously in 2DEGs with two [27,28] or more [29] intersubband transitions. In systems with many occupied subbands, Coulomb interactions can induce coherence between multiple intersubband resonances, leading to a high-energy collective mode that concentrates most of the spectral weight. Indeed, in the high-density case in Fig. 5, we see a sharp peak arises at the energy 1.1 eV beyond the upper bound of the intersubband splittings. This is an excitation of plasmonic character which arises from Coulomb coupling of a large number of intersubband transitions into a single collective mode. At medium density, the collective mode is just beginning to emerge from the coupled intersubband transitions, but is not fully separated. At low density, the spectrum is only slightly shifted towards higher energy. The peaks centered at low frequencies are strongly suppressed at all densities.

VI. SUMMARY AND CONCLUSIONS

We report on a theoretical model study of the optical conductivity of t_{2g} 2DEGs formed at perovskite oxide surfaces and interfaces. The detailed properties of these low-dimensional electron systems are difficult to predict theoretically because of the important role played in their properties by nonlocal and nonlinear dielectric screening and by structural distortions and defects. This study is motivated by the potential value of spectral and sum-rule information from optical characterization for verification and refinement of models of t_{2g} 2DEG properties.

We find that the in-plane optical conductivity is very strongly dominated by approximately independent Drude peak contributions coming from all bands, irrespective of their t_{2g}-orbital character and of the degree to which they are confined at the interface. Unlike the dc conductivity, the Drude weight, obtained by integrating the Drude peak over frequency, is independent of the unknown scattering times of the various bands. Measuring the Drude weight of the t_{2g} 2DEG can provide an estimate of the total 2D carrier density that is complementary to the one provided by Hall effect measurements. Neither measurement is definitive on its own, since the Hall effect is simply related to carrier density only in single-band systems, and the Drude weight of a band depends both on its carrier density and its effective mass. We have calculated the effective masses which should be used in combination with Drude weight measurements to infer the carrier density.

The in-plane conductivity also has features associated with intersubband transitions. These are weak unless spin-orbit interactions significantly hybridize t_{2g} electrons with different orbital character, but would be very valuable in characterizing the subband structure if they could be detected. In the

model calculations we have performed, the primary source of hybridization is atomic-like spin-orbit interactions which will normally have the strongest impact. Because Rashba [13] spin-orbit interactions, which we have not specifically included in the present calculations, are necessarily momentum and gate-voltage dependent, they could provide a gate-tunable source of spin-orbit coupling. By providing weight to intersubband features in the in-plane conductivity, tunable Rashba interactions could enhance the value of in-plane current response measurements.

Unlike its in-plane counterpart, perpendicular-to-plane optical conductivity measurements should reveal valuable spectroscopic information. Their interpretation is, however, complicated by depolarization effect which implies that spectral features cannot be immediately identified with intersubband transition energies. The coupling between different intersubband transitions shifts spectral features to higher energies and suppresses low-energy transition features. In 2DEGs with a large enough 2D density we predict that a plasmon-like collective mode, resulting from Coulomb-coupling induced in-phase oscillation of a large number of intersubband transitions, appears above the highest transition energies and carries most of the spectral weight.

Based on our study we also conclude that the influence of gates, particularly the influence of back gates on ellipsometry, might be helpful in assigning features to particular transitions in the t_{2g} 2DEG. When the t_{2g} carrier density is reduced by a back gate [14] it has the effect of increasing the electric field deep in the substrate, which has a particularly strong influence on the weakly confined states which are otherwise present, sharply increasing the smallest subband splittings, decreasing the number of partially occupied subbands, and increasing spatial overlap between occupied and empty subbands. We can expect that broad tails in optical response will sharpen into discrete features which can be assigned on the basis of their spectral response to back-gate voltages, and that the plasmon-like collective mode will be suppressed.

ACKNOWLEDGMENTS

This work was supported by NSF DMR 1122603 and by the Robert A Welch Foundation Grant TBF1473.

[1] D. G. Schlom, L. Q. Chen, X. Pan, A. Schmehl, and M. A. Zurbuchen, J. Am. Ceram. Soc. **91**, 2429 (2008).
[2] J. Son, P. Moetakef, B. Jalan, O. Bierwagen, N. J. Wright, R. Engel-Herbert, and S. Stemmer, Nat. Mater. **9**, 482 (2010).
[3] A. Ohtomo and H. Y. Hwang, Nature (London) **427**, 423 (2004).
[4] A. Brinkman, M. Huijben, M. van Zalk, J. Huijben, U. Zeitler, J. C. Maan, W. G. van der Wiel, G. Rjinders, D. H. A. Blank, and H. Hilgenkamp, Nat. Mater. **6**, 493 (2007).
[5] N. Reyren, S. Thiel, A. D. Caviglia, L. Fitting Kourkoutis, G. Hammerl, C. Richter, C. W. Schneider, T. Kopp, A. S. Ruetschi, D. Jaccard, M. Gabbay, D. A. Muller, J.-M. Triscone, and J. Mannhart, Science **317**, 1196 (2007).
[6] L. Li, C. Richter, J. Mannhart, and R. C. Ashoori, Nat. Phys. **7**, 762 (2011); D. A. Dikin, M. Mehta, C. W. Bark, C. M. Folkman, C. B. Eom, and V. Chandrasekhar, Phys. Rev. Lett. **107**, 056802 (2011); J. A. Bert, B. Kalisky, C. Bell, M. Kim, Y. Hikita, H. Y. Hwang, and K. A. Moler, Nat. Phys. **7**, 767 (2011); P. Moetakef, J. R. Williams, D. G. Ouellette, A. P. Kajdos, D. Goldhaber-Gordon, S. J. Allen, and S. Stemmer, Phys. Rev. X **2**, 021014 (2012).
[7] J. Mannhart and D. G. Schlom, Science **327**, 1607 (2010); J. Mannhart, D. H. A. Blank, H. Y. Hwang, A. J. Millis, and J.-M. Triscone, MRS Bull. **33**, 1027 (2008).
[8] A. Ohtomo, D. A. Muller, J. L. Grazul, and H. Y. Hwang, Nature (London) **419**, 378 (2002).
[9] P. Moetakef, T. A. Cain, D. G. Ouellette, J. Y. Zhang, D. O. Klenov, A. Janotti, C. G. Van de Walle, S. Rajan, S. J. Allen, and S. Stemmer, Appl. Phys. Lett. **99**, 232116 (2011); P. Moetakef, J. Y. Zhang, A. Kozhanov, B. Jalan, R. Seshadri, S. J. Allen, and S. Stemmer, *ibid.* **98**, 112110 (2011).
[10] K. Ueno, S. Nakamura, H. Shimotani, A. Ohtomo, N. Kimura, T. Nojima, H. Aoki, Y. Iwasa, and M. Kawasaki, Nat. Mater. **7**, 855 (2008); Y. Lee, C. Clement, J. Hellerstedt, J. Kinney, L. Kinnischtzke, X. Leng, S. D. Snyder, and A. M. Goldman, Phys. Rev. Lett. **106**, 136809 (2011); M. Lee, J. R. Williams, S. Zhang, C. D. Frisbie, and D. Goldhaber-Gordon, *ibid.* **107**, 256601 (2011).
[11] B. Jalan, S. J. Allen, G. E. Beltz, P. Moetakef, and S. Stemmer, Appl. Phys. Lett. **98**, 132102 (2011).
[12] K. Ueno, S. Nakamura, and H. Shimotani, Nature Nanotechnol. **6**, 408 (2011); P. D. C. King, R. H. He, T. Eknapakul, P. Buaphet, S. K. Mo, Y. Kaneko, S. Harashima, Y. Hikita, M. S. Bahramy, C. Bell, Z. Hussain, Y. Tokura, Z. X. Shen, H. Y. Hwang, F. Baumberger, and W. Meevasana, Phys. Rev. Lett. **108**, 117602 (2012).
[13] A. D. Caviglia, M. Gabay, S. Gariglio, N. Reyren, C. Cancellieri, and J.-M. Triscone, Phys. Rev. Lett. **104**, 126803 (2010); A. Fete, S. Gariglio, A. D. Caviglia, J.-M. Triscone, and M. Gabay, Phys. Rev. B **86**, 201105(R) (2012); H. Nakamura, T. Koga, and T. Kimura, Phys. Rev. Lett. **108**, 206601 (2012); Z. Zhong, A. Toth, and K. Held, Phys. Rev. B **87**, 161102(R) (2013); G. Khalsa, B. Lee, and A. H. MacDonald, *ibid.* **88**, 041302 (2013).
[14] G. Khalsa and A. H. MacDonald, Phys. Rev. B **86**, 125121 (2012).
[15] M. Stengel, Phys. Rev. Lett. **106**, 136803 (2011).
[16] T. Ando, A. B. Fowler, and F. Stern, Rev. Mod. Phys. **54**, 437 (1982).
[17] G. Harbeke, Phys. Scr. T **29**, 135 (1989).
[18] L. C. West and S. J. Eglash, Appl. Phys. Lett. **46**, 1156 (1985).
[19] A complementary theoretical paper with a similar motivation appeared as we were preparing this paper for publication: S. Y. Park and A. J. Millis, Phys. Rev. B **87**, 205145 (2013). These authors made an effort to connect more directly with ellipsometry, and in particular estimated the interaction induced shifts in intersubband transition energies. Our paper focuses more on features associated with the weak coupling between t_{2g} bands which can make optical characterization more useful, and accounts for their finite heavy masses which often play an essential role.
[20] R. Kubo, J. Phys. Soc. Jpn. **12**, 570 (1957).

[21] G. Mahan, *Many-Particle Physics*, 3rd ed. (Kluwer Academic/Plenum, New York, 2010).

[22] S. J. Allen, B. Jalan, S. B. Lee, D. G. Ouellette, G. Khalsa, J. Jaroszynski, S. Stemmer, and A. H. MacDonald, Phys. Rev. B **88**, 045114 (2013).

[23] Z. Q. Liu, C. J. Li, W. M. Lu, X. H. Huang, Z. Huang, S. W. Zeng, X. P. Qiu, L. S. Huang, A. Annadi, J. S. Chen, J. M. D. Coey, T. Venkatesan, and Ariando, Phys. Rev. X **3**, 021010 (2013).

[24] J. L. M. van Mechelen, D. van der Marel, C. Grimaldi, A. B. Kuzmenko, N. P. Armitage, N. Reyren, H. Hagemann, and I. I. Mazin, Phys. Rev. Lett. **100**, 226403 (2008); R. Cowley, Phys. Rev. **134**, A981 (1964).

[25] A. Janotti, D. Steiauf, and C. G. Van de Walle, Phys. Rev. B **84**, 201304 (2011); Y. J. Chang, G. Khalsa, L. Moreschini, A. L. Walter, A. Bostwick, K. Horn, A. H. MacDonald, and E. Rotenberg, *ibid.* **87**, 115212 (2013).

[26] S. J. Allen, D. C. Tsui, and B. Vinter, Solid State Commun. **20**, 425 (1976).

[27] J. Li and C. Z. Ning, Phys. Rev. Lett. **93**, 087402 (2004).

[28] R. J. Warburton, C. Gauer, A. Wixforth, J. P. Kotthaus, B. Brar, and H. Kroemer, Phys. Rev. B **53**, 7903 (1996).

[29] A. Delteil, A. Vasanelli, Y. Todorov, C. Feuillet Palma, M. Renaudat St-Jean, G. Beaudoin, I. Sagnes, and C. Sirtori, Phys. Rev. Lett. **109**, 246808 (2012).